Electrochemical Studies of Polynucleotide Binding and Oxidation by Metal Complexes: Effects of Scan Rate, Concentration, and Sequence

Mark F. Sistare, Rebecca C. Holmberg, and H. Holden Thorp*

Department of Chemistry, University of North Carolina, Chapel Hill, North Carolina 27599-3290

Received: August 19, 1999; In Final Form: October 5, 1999

The electrocatalytic oxidation of guanine in DNA and oligonucleotides by $Ru(bpy)_3^{3+/2+}$ was investigated using cyclic voltammetry (CV) and chronoamperometry (CA) (bpy = 2,2′-bipyridine). Oxidation of $Ru(bpy)_3^{2+}$ to the Ru(III) form at tin-doped indium oxide (ITO) electrodes in the presence of DNA produces catalytic current due to the oxidation of guanine by Ru(III). CA traces of $Ru(bpy)_3^{2+}$ with calf thymus DNA at high salt concentration (50 mM sodium phosphate + 700 mM NaCl) give a single kinetic process with a rate constant of $3500 \pm 300\ M^{-1}\ s^{-1}$ that is independent of DNA concentration and similar to values determined previously by fitting CV data under the same conditions. Under low salt conditions (50 mM sodium phosphate + 0 mM NaCl), the CA data show two linear regions that give rate constants of 2.7×10^4 and $6 \times 10^5\ M^{-1}\ s^{-1}$. Digital simulation of CV data at low salt requires a careful accounting for the binding of the metal complex to the DNA polyanion, which can be accomplished using binding constants that are independently determined. This analysis gives rate constants that are independent of DNA concentration and range from 2.3×10^5 to $1.4 \times 10^6\ M^{-1}\ s^{-1}$ as the scan rate is increased from 25 to 250 mV/s. The variation in rate constant with scan rate can be attributed to the two kinetic processes observed in the CA results. Resolution of $Ru(bpy)_3^{2+}$ into the Δ and Λ stereoisomers showed that the two kinetic processes were not due to the stereoisomerism. Satisfactory fitting of the CV data requires addition of a second electron-transfer step from the oxidized guanine to Ru(III); this rate constant was always less than 1% of the rate constant for the first homogeneous electron transfer. In addition, the fitting at low salt requires accounting for the density of guanines in the DNA sequence. Calf thymus DNA is 20% guanine; however, the fitting shows that binding of the mediator by at least 60% of the nucleotides produces catalytic turnover. Oligonucleotides containing a single guanine gave similar rate constants to those observed by CV and CA on calf thymus DNA, and the fitting suggested that binding of the mediator by 5−10 of the 30 nucleotides (defined as "active binding sites") in the oligomer produced catalyst cycling. Thus, the electron is able to transfer to a mediator that is bound in a region that spans 2.5−5 base pairs and contains the oxidized guanine. The number of "active binding sites" increased predictably with the number of guanines in the sequence, ranging from 15% to 33% of the total nucleotides for a 15-mer duplex with one guanine to 75−100% for a 15-mer duplex with six guanines. Decreasing the salt concentration enhances the catalytic current both by increasing the number of active binding sites by a factor of 5−10 and by increasing the intrinsic oxidation rate by an order of magnitude.

Electron-transfer reactions of oligonucleotides are a subject of intense interest and investigation.[1−6] The guanine base is the most facile electron donor and has been used as a convenient probe of the dynamics of DNA electron transfer both parallel and perpendicular to the long axis of the DNA double helix.[1,7−11] Electrochemical techniques are difficult to apply to guanine electron transfer in DNA polymers, especially for mechanistic studies, because the high molecular weight reduces the diffusion coefficient and the three-dimensional structure of DNA protects the guanine from oxidation and lowers the electron-transfer rate.[12,13] Electrochemical techniques can be used directly to detect guanine in DNA with high sensitivity; however, these approaches generally rely on adsorption of the DNA to carbon paste or mercury electrodes.[14−16] An alternative approach is to utilize an electrode material that itself catalyzes DNA oxidation; this approach also provides high sensitivity but little mechanistic information.[17]

We have developed an approach for studying guanine oxidation in room temperature, fluid solution using mediators based on $Ru(bpy)_3^{2+}$ (bpy = 2,2′-bipyridine).[12,13,18] In this system, DNA is dissolved in the buffer of choice and electrons are shuttled from guanine to the electrode via the $Ru(bpy)_3^{3+/2+}$ couple, which exhibits a relatively high diffusion coefficient and a fast heterogeneous electron-transfer rate. Addition of DNA to solutions of $Ru(bpy)_3^{2+}$ produces current enhancements in the cyclic voltammogram (CV) that can be ascribed to the oxidation of guanine in DNA by Ru(III) to generate Ru(II) and complete a catalytic cycle. When tin-doped indium oxide (ITO) is used as the electrode material, the adsorption of DNA to the electrode and the current due to direct guanine oxidation are negligible. The acquired voltammetric responses can be digitally simulated to determine the kinetic parameters for guanine oxidation.[19,20] At relatively high ionic strength (>700 mM NaCl), binding of $Ru(bpy)_3^{3+/2+}$ to DNA can be neglected and rate constants in the range $10^3-10^4\ M^{-1}\ s^{-1}$ can be determined by digital simulation of voltammograms as well as cyclic square wave voltammetry and stopped-flow spectrophotometry.[20] At lower salt concentrations, the electrostatic binding of $Ru(bpy)_3^{3+/2+}$ to the DNA polyanion becomes important and digital simulation requires more extensive mechanisms to fit the data.[20] The

10.1021/jp992940f CCC: $18.00
Published on Web 11/11/1999

apparent rate constants at low salt concentration are approximately an order of magnitude higher, representing an increase in the effective DNA concentration brought about by binding of the catalyst.

Here, we consider in more detail the impact of DNA binding of $Ru(bpy)_3^{3+/2+}$ on the electrochemical response and associated electron-transfer rate constants. Our earlier fitting did not treat the DNA sequence explicitly and therefore ignored the subtleties associated with binding events that did not lead to catalyst turnover.[20] We now treat the possibility that some binding events produce a $Ru(bpy)_3^{3+}$·DNA configuration where guanine oxidation does not occur. These nonproductive binding events presumably involve configurations with large guanine−Ru distances. This treatment suggests that binding of the $Ru(bpy)_3^{3+}$ in a 2.5−5 base pair region containing a guanine leads to catalyst turnover. The kinetics of the oxidation process are biphasic, which is evident in both chronoamperometry (CA) experiments and in the scan rate dependence of CV.

Experimental Section

DNA. Calf thymus DNA, sodium salt was obtained from Sigma (St Louis, MO) and was used as received. Stock solutions were prepared by slowly dissolving the solid DNA in buffer and stored at 4 °C. The nucleotide concentration was determined spectrophotometrically ($\epsilon_{260} = 6600\ M^{-1}\ cm^{-1}$, per nucleotide).[21] Synthetic oligonucleotides were obtained either from the UNC Department of Pathology or the Lineberger Comprehensive Cancer Center Nucleic Acids Core Facility and purified either by HPLC, filtration on a Centricon 3 (Amicon, Bedford, MA) 3000 MW cutoff filter, or two successive ethanol precipitation steps. Oligonucleotide solution concentrations were determined spectrophotometrically per strand.[22] Oligonucleotide strands were designed such that all guanines were located on a target strand; double-stranded samples were obtained by heating the DNA in the presence of excess complementary strand to 90 °C and cooling slowly over 2 h. All electrochemical experiments were performed with double-stranded DNA, unless otherwise stated.

Reagents. Deionized water was obtained by passing in-house distilled water though a Milli-Q (18 Ω) deionizing system (Millipore Corporation, Bedford, MA) and was used for the preparation of all aqueous solutions. Sodium phosphate salts and sodium chloride were obtained from Mallinckrodt (Paris, KY) and used as received. $Ru(bpy)_3^{2+}$ was obtained from Aldrich (Milwaukee, WI) and recrystallized once in acetonitrile prior to use. The concentration of the $Ru(bpy)_3^{2+}$ solution was determined from absorbance measurements using $\epsilon_{452} = 14\,600\ M^{-1}\ cm^{-1}$.[23] All other reagents were obtained from Aldrich and used as received.

The isomers of $Ru(bpy)_3^{2+}$ were separated by chiral eluent chromatography according to the procedure of Keene et al.[24] The eluted enantiomers were isolated as the PF_6^- salts by addition of NH_4PF_6 to the tartrate buffer. The isolated PF_6^- salts were then dissolved in acetone and converted to the chloride salts by addition of tetrabutylammonium chloride.

Electrodes. ITO electrodes were obtained from Delta Technologies, Ltd. (Stillwater, MN). All ITO electrodes were cleaned by sonication in Alconox, 2-propanol, and deionized water (twice), each step for 15 min, similar to the method introduced by Armstrong et al.[25] Because extended exposure to water seems to degrade the ITO surface, electrodes were allowed to air-dry following the last sonication step and stored in a covered container until use. The electrodes were electrochemically conditioned prior to data collection by scanning the buffer solution at the intended scan rate until consecutive scans were identical, typically eight cycles.

Electrochemistry. All electrochemical experiments were performed on either an EG&G PAR 273A or a BAS 100B/W potentiostat controlled by a PC. The electrochemical cell assembly, in which the ITO working electrode forms the bottom of the cell, has been described previously.[26] The reference electrode was a commercially available Ag/AgCl (3.0 M KCl) electrode obtained from Cypress Systems (Lawrence, KS). The counter electrode, a 22-gauge platinum wire (Alfa, Ward Hill, MA), was wrapped around the shaft of the reference electrode. For CA, the potential was stepped from 0.85 to 1.3 V to minimize double layer charging effects, and the low pass filter was disabled to maximize instrument response. CVs were collected over a scan rate range of 25−250 mV/s with an enabled 5.3 Hz pass filter. A CV of the buffer without metal complex or nucleic acid was subtracted from all of the voltammograms shown and analyzed here.

Digital Simulation. Digital simulations were performed using the DigiSim software package (Bioanalytical systems, West Lafayette, IN).[27] The diffusion coefficients used were $6.0 \times 10^{-6}\ cm^2/s$[19] for $Ru(bpy)_3^{2+}$ and $2.0 \times 10^{-7}\ cm^2/s$[28] for calf thymus DNA. Oligonucleotide diffusion coefficients were calculated by assuming rigid rod behavior.[29,30] For all of the homogeneous binding steps in the mechanism, the forward rate constant was set to the diffusion-limited value of $1.0 \times 10^9\ M^{-1}\ s^{-1}$. The binding constants used for $Ru(bpy)_3^{2+/3+}$ were $K^{2+} = 700\ M^{-1}$[31,32] and $K^{3+} = 3500\ M^{-1}$.[28] The reduction potential of the $Ru(bpy)_3^{3+}$, the electrode area, and the heterogeneous electron-transfer rate constant were obtained by fitting the voltammogram of $Ru(bpy)_3^{2+}$ in the absence of DNA. Further, since there is a small rate of spontaneous conversion of $Ru(bpy)_3^{3+}$ to $Ru(bpy)_3^{2+}$ alone in solution,[33] this rate was also determined by simulating the voltammogram in the absence of DNA.

Results

Chronoamperometry of Calf Thymus DNA. As stated above, our studies of the $Ru(bpy)_3^{2+}$/DNA catalytic reaction have centered on two regimes: a high-salt (>700 mM Na^+) regime where binding of $Ru(bpy)_3^{2+}$ to DNA can be neglected, and a low salt (88 mM Na^+) regime where the binding must be accounted for.[19,20] In the high salt case, second-order rate constants have been obtained directly for the reaction of $Ru(bpy)_3^{3+}$ with calf thymus DNA from CV, stopped-flow spectrophotometry, and square-wave voltammetry.[19,20] We have now examined the kinetics of this reaction under high salt conditions by chronoamperometry (CA). The theory for studying generalized catalytic systems with CA has been developed,[34−36] although only for pseudo-first-order systems where a single catalytic step follows a reversible electron-transfer step. The results here were analyzed using this existing treatment for the pseudo-first-order case to obtain an *apparent* second-order rate constant for the reaction of $Ru(bpy)_3^{3+}$ with DNA.

CA results for a reversible electron transfer are described by the Cottrell equation,[34,36]

$$i = \frac{nFAD_o^{1/2}C_o^*}{\pi^{1/2}t^{1/2}} \quad (1)$$

where i is the current response, n is the number of electrons transferred per mole of the redox couple, F is the Faraday constant, D is the diffusion coefficient, and C_o^* is the bulk concentration of the redox couple. For a catalytic reaction in

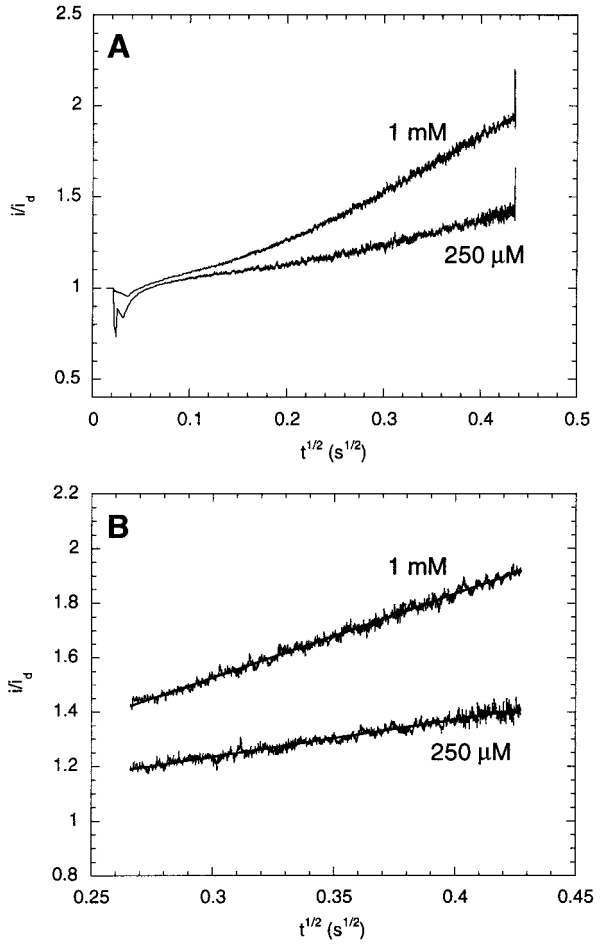

Figure 1. Ratio of CA data at high salt (50 mM phosphate buffer + 700 mM NaCl) for $Ru(bpy)_3^{2+}$ (50 μM) alone (i) and in the presence of 250 μM or 1 mM DNA (i_d): (A) entire time trace; (B) pure kinetic region showing linear fit as a solid line.

the $E_{rev}C'_{irrev}$ case (in which the nonelectroactive species is in large excess), the ratio of catalytic current to current in the absence of substrate is[34]

$$\frac{i}{i_d} = \lambda^{1/2}\left[\pi^{1/2} erf(\lambda^{1/2}) + \frac{e^{-\lambda}}{\lambda^{1/2}}\right] \quad (2)$$

In eq 2, i_d is the limiting current for the heterogeneous electron-transfer reaction in the absence of the following catalytic reaction, and λ accounts for the catalytic reaction as follows:

$$\lambda = k'C_Z^* t \quad (3)$$

where k' is the second-order rate constant and C_Z^* is the concentration of the substrate. At early times, $i/i_d = 1$. At longer times ($\lambda > 1.5$) the error function approaches unity, and the last term approaches zero, defining the pure kinetic region. In this region, eq 2 reduces to the following:

$$\frac{i}{i_d} = \pi^{1/2}\lambda^{1/2} \quad (4)$$

A plot of i/i_d versus $t^{1/2}$ is therefore linear at long times with a slope equal to $(\pi k' C_Z^*)^{1/2}$.

Figure 1A shows the chronoamperometric response for $Ru(bpy)_3^{2+}$-mediated oxidation of calf thymus DNA in high ionic strength buffer (50 mM sodium phosphate + 700 mM NaCl, $[Na^+]$ = 788 mM). The apparent second-order rate constants (k') were obtained from the slope at long times (Figure 1B) and are given in Table 1. As expected, the rate constants do not exhibit a systematic dependence on guanine concentration, and the precision improves at higher guanine concentrations due to larger values of i/i_d. The mean value calculated for the rate constant under high-salt conditions is 3500 ± 300 M^{-1} s^{-1}, approximately a factor of 3 lower than that found by CV and digital simulation under the same ionic strength conditions.[19,20] Origins of this difference will be discussed below.

TABLE 1: Second-Order Rate Constants for Oxidation of Calf Thymus DNA by $Ru(bpy)_3^{3+}$ Determined by CA

$[Na^+]$ (mM)	$[DNA]_{np}$ (μM)	phase	slope	$10^{-3} \times k_2$ (M^{-1} s^{-1})
788	1250		1.7 ± 0.4	3.9 ± 1.5
	2500		2.3 ± 0.2	3.3 ± 0.7
	5000		3.2 ± 0.2	3.4 ± 0.4
88	1250	fast	23 ± 1	680 ± 20
		slow	4.8 ± 0.2	30 ± 2
	2500	fast	34 ± 5	760 ± 200
		slow	6.6 ± 0.2	27 ± 1
	5000	fast	37 ± 3	440 ± 60
		slow	8.8 ± 0.2	25 ± 1

A similar analysis was attempted for calf thymus DNA under low ionic strength conditions, where electrostatic binding is important. Figure 2A shows the chronoamperometric response in sodium phosphate buffer at an ionic strength of 50 mM ($[Na^+]$ = 88 mM). When electrostatic binding is important, the curve shows two linear regimes: one fast regime at early times and a slower regime at later times. These two linear regimes were interpreted as two phases of the catalytic reaction, and apparent second-order rate constants were determined from the best fit straight lines at early and late times. The rate constants obtained for the fast and slow phases are shown in Table 1. The apparent rate constant for the slow phase has an average value of $(2.7 \pm 0.2) \times 10^4$ M^{-1} s^{-1}, about an order of magnitude larger than in the high ionic strength case where binding is unimportant (i.e., Figure 1). A similar relationship was observed between rate constants obtained from simulation of CVs under high and low ionic strength conditions.[20] The fast phase exhibits an average rate constant of $(6 \pm 1) \times 10^5$ M^{-1} s^{-1}, which is approximately 20-fold faster than the slow phase. Inspection of Figure 2 shows that the fast phase is significant but probably accounts for much less than half of the total catalytic current.

CV of Calf Thymus DNA. Because the high ionic strength case where binding of $Ru(bpy)_3^{3+/2+}$ to DNA can be neglected has been worked out in detail for CV,[19] included here are only the cases where electrostatic binding is important. The mechanism used to describe this case is shown in Scheme 1. This entire scheme must be applied in these simulations because the DNA, and therefore bound mediator, has a diffusion coefficient that is an order of magnitude smaller than that for the free mediator. Here we use the same mechanism as that in our previous study,[20] except that the fitting methodology has been changed to incorporate the concept of territorial binding. The theory for territorial binding of cations to DNA has been described in detail by Manning and Record[37−39] and shown by our group to apply to studies of polypyridyl complexes and DNA,[31,40] including the description of electrochemical responses.[28] If a polyelectrolyte is described by a cylinder, a counterion is said to participate in territorial binding when it is localized within a second cylinder that is coaxial with the polyelectrolyte cylinder. We find that the territorial binding model improves the fitting for calf thymus DNA but is more important in fitting data for known sequences containing a relatively low number of guanines, as described later.

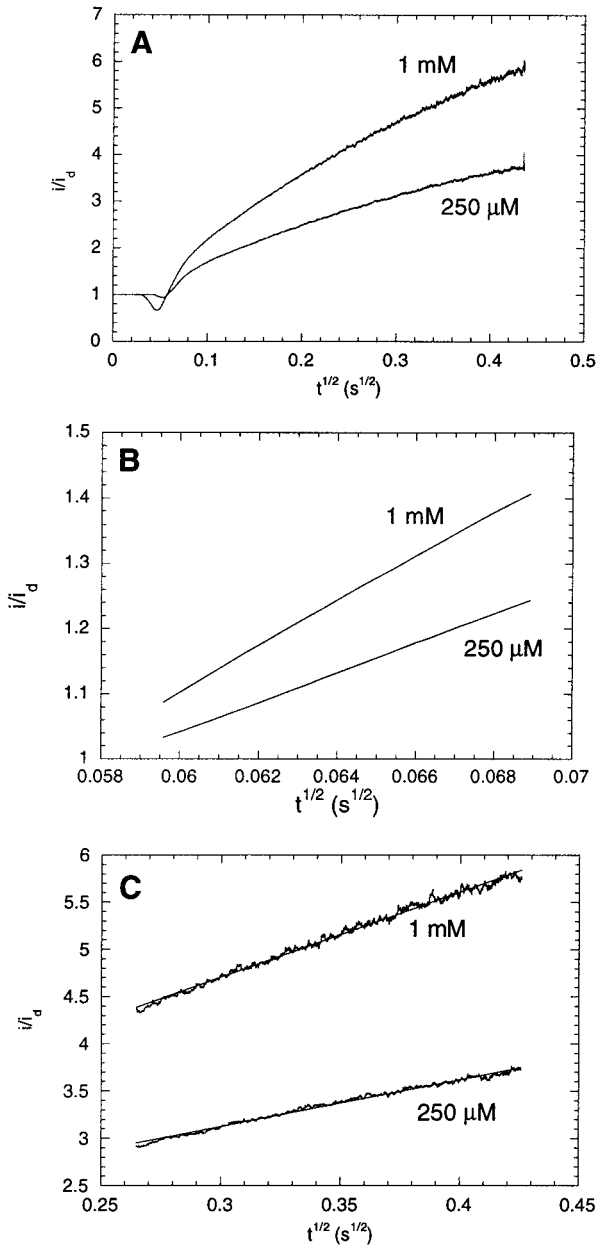

Figure 2. Ratio of CA data at low salt (50 mM phosphate buffer + no added NaCl) for $Ru(bpy)_3^{2+}$ (50 μM) alone (i) and in the presence of 250 μM or 1 mM DNA (i_d): (A) entire time trace; (B) fast phase showing linear fit as a solid line; (C) slow phase showing linear fit as a solid line.

The territorial binding model suggests that a mediator can, while bound, diffuse some finite distance along the DNA helix, which may bring the metal complex close enough to a guanine for electron transfer to occur. Guanines within the range of the bound mediator are herein defined as lying in "active binding sites" (see Figure 3). Bard et al. have shown that it is difficult to distinguish between mediator migration on the strand or dissociation and rebinding of the mediator during a single sweep, so we do not attempt such a distinction here.[41] As we have discussed previously,[20] a dichotomy that must be addressed in the analysis using Scheme 1 is that the concentration of guanine is the parameter that controls the rate constant for oxidation; however, the binding equilibria are governed by the total concentration of nucleotides. Thus, the model must account for nucleotides that bind the metal complex but are not oxidized. We have addressed this dichotomy by converting DNA concentration to the concentration of active binding sites, which is

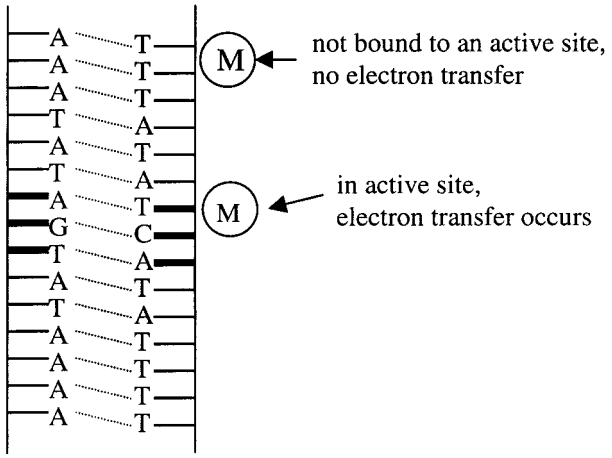

Figure 3. Cartoon of binding model used to determine the number of active sites. The picture shows the scenario where there are six active sites (shown as bold lines). One $Ru(bpy)_3^{3+}$ (M) is bound at an active site and can undergo electron transfer while the other is bound far from a guanine and will not undergo electron transfer.

SCHEME 1

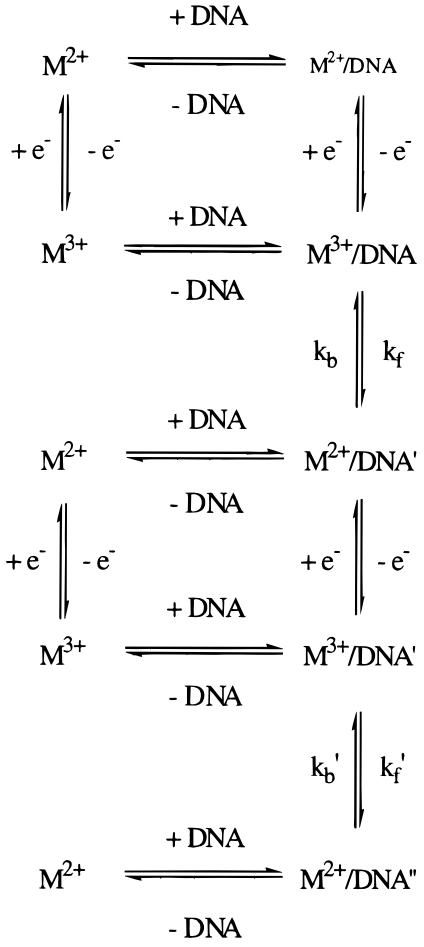

the total nucleotide concentration divided by a factor that reduces the total number of nucleotides to the number of sites where a bound metal complex will be able to abstract an electron. The binding constant is then corrected by multiplying the known binding constants per nucleotide, 700 M^{-1} for $Ru(bpy)_3^{2+}$ and 3500 M^{-1} for $Ru(bpy)_3^{3+}$,[28,31,32] by the total number of nucleotides and dividing by the number of active sites, thereby giving the correct concentration of total bound metal complex. We have shown that this approximation is valid as long as the

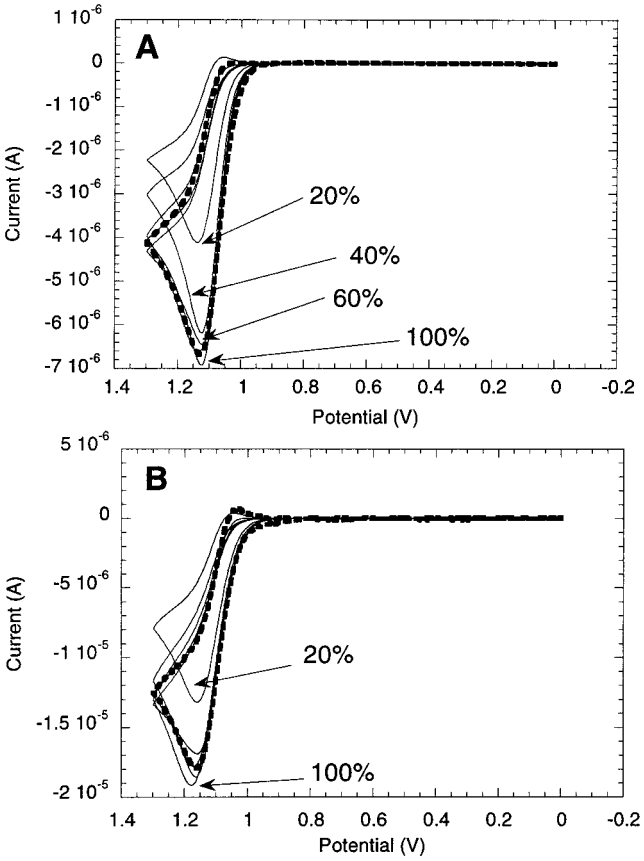

Figure 4. CVs of calf thymus DNA (500 μM nucleotides) with $Ru(bpy)_3^{2+}$ (50 μM) showing experimental voltammograms (dashed) and simulations (solid) calculated for 20%, 40%, 60%, 80%, and 100% active nucleotides. (A) Scan rate = 25 mV/s. Simulations for 60% and 80% are very close to the experimental voltammogram. (B) Scan rate = 250 mV/s. Simulations for 40%, 60%, and 80% are very close to the experimental voltammogram.

binding is described by a weak binding isotherm,[20] which is expected for a complex like $Ru(bpy)_3^{2+}$ whose binding is driven primarily by electrostatics. As we will describe below, the number of active binding sites is determined empirically from the parameters that best-fit the data.

Simulations in which Scheme 1 is employed return first-order rate constants for the electron-transfer step. A second-order rate constant is desirable, however, since comparison to the results obtained in the high ionic strength case is warranted. The steady-state approximation provides a relationship between the first-order and second-order rate constants as shown below,[20]

$$k_2 = k_1 \frac{K_b^{3+}}{K_b^{3+}[\mathrm{DNA}_{(G)}] + 1} \qquad (5)$$

The binding constant and DNA concentration used for this relationship must account for binding at all bases but oxidation only at guanine. As discussed above, the binding constant per nucleotide is therefore multiplied by the reciprocal of the fraction of nucleotides that are guanine in the double-stranded oligomer and the concentration is entered in terms of guanine, termed $[DNA_{(G)}]$.

Figure 4 shows a representative CV of $Ru(bpy)_3^{2+}$-mediated calf thymus DNA oxidation overlaid with a set of simulations in which the fraction of active binding sites is varied from 20%, the actual guanine content in calf thymus DNA,[21] to 100%. If 20% of the sites were active, then the metal complex could abstract an electron only if it were bound at a guanine nucleotide. The other extreme is represented by the case where the nucleotides are 100% active and every binding event leads to electron transfer, regardless of where the metal complex is bound in the sequence. As shown in Figure 4, simulations that model 20% and 40% active sites did not fit the data well. The failure of the low active site model to fit the data is more pronounced at lower scan rates. For the 250 mV/s case, a fraction of 40% is nearly able to account for most of the anodic current, and the 100% model actually overestimates the anodic current by a small amount.

TABLE 2: Simulated Rate Constants for Calf Thymus DNA Oxidation by $Ru(bpy)_3^{3+}$

scan rate (mV/s)	$k \times 10^{-5}$ (M^{-1} s^{-1}), 60%[a]	$k \times 10^{-5}$ (M^{-1} s^{-1}), 80%[b]	$k \times 10^{-5}$ (M^{-1} s^{-1}), 100%[c]
25	2.9 ± 0.3	2.2 ± 0.1	1.7 ± 0.1
50	3.6 ± 0.3	2.3 ± 0.2	2.3 ± 0.1
100	5.2 ± 0.5	4.1 ± 0.2	3.5 ± 0.1
250	14 ± 4	12 ± 3	7 ± 1

[a] Determined by fitting of CVs as in Figure 2 with a model where binding at 60% of the nucleotides leads to electron transfer. First-order rate constants returned from the fitting were converted to second-order rate constants according to eq 4. Error limits are from multiple trials at different DNA concentrations. [b] Determined from fitting CVs with 80% active nucleotides. [c] Determined from fitting CVs with 100% active nucleotides.

Shown in Table 2 are the second-order rate constants determined by fitting the CV of calf thymus DNA with $Ru(bpy)_3^{2+}$ at low ionic strength. The results are shown for fitting with models using 60%, 80%, and 100% active sites at a series of scan rates. As with the CA, there was little dependence of the second-order rate constant on guanine concentration. The values in Table 2 are averages taken over a series of DNA concentrations. At low scan rates, the rate constants are relatively low and do not vary significantly with the model (60%, 80%, or 100%) chosen. The rate constant determined at 25 mV/s (the average value is 2.3×10^5 M^{-1} s^{-1}) is about 10 times faster than that of the slow phase of the CA (2.7×10^4 M^{-1} s^{-1}) in Figure 2. This difference probably occurs because in the CV experiment, both the fast and slow phases contribute to the apparent rate of catalyst turnover. At fast scan rates, there is a stronger dependence on the model chosen, and the lower fractions of active sites appear to fit the data better (Figure 4). The appropriateness of lower active sites at faster scan rates is expected, since there is less time for catalysis and therefore less time for metal complexes to sample all of the available guanine donors. Accordingly, higher rate constants are observed at lower active site fractions, because a faster reaction is needed to account for the same amount of catalyst turnover with lower effective substrate concentrations. For similar reasons, the rate constants determined at higher scan rates are generally higher because the shorter reaction time causes sampling of a smaller fraction of the entire time trace shown in the CA results in Figure 2. As the scan rate is increased, the fast process contributes more to the apparent rate constant, and the single rate constant returned from the CV simulations increases. The maximum rate constant determined at 250 mV/s (1.4×10^6 M^{-1} s^{-1}) is only about a factor of 2 faster than that determined from the earliest time points by CA.

As shown in Scheme 1, the model used to fit the CV contains a second electron-transfer step where DNA molecules that have been oxidized by one electron (DNA′) are oxidized by a second electron (to produce DNA″). This second electron transfer is well supported by studies on the molecular mechanisms of guanine redox chemistry,[5,6,42] which show that the one-electron

oxidation product proceeds on to form 8-oxo-guanine.

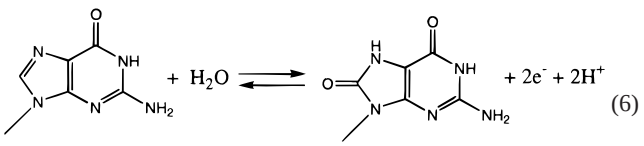

(6)

The accumulated evidence suggests that the first electron transfer occurs rapidly to give a radical cation that is rapidly deprotonated.[43] The second step presumably involves formation of the new C═O bond at the imidazole carbon and would be expected to proceed much more slowly. We have found that better fits of the CV are obtained when a second electron transfer (i.e., M3/DNA′ → M2/DNA″) is included in the model. However, when an appropriate number of active sites is used, the rate constant for the second electron transfer is 1% or less of that for the first electron transfer. In the simulations that produced all of the rate constants reported here, this condition was satisfied. Thus, neglecting the contribution of the second electron transfer in the steady-state approximation does not significantly alter the second-order rate constant calculated for the first electron transfer according to eq 5.

There are several predictions that can be made from the results presented thus far. CV is not the ideal technique for analyzing biphasic reactions, because only a fraction of the reaction course is sampled at any given scan rate;[44] however, the catalytic effect is much easier to detect in CV than in any other technique. At slow scan rates, the apparent rate constant should approach that of the limiting slow component in the CA. A first prediction that can be made is that at sufficiently fast scan rates, the rate constant returned from fitting CV would approach an upper limit determined by the fast component in Figure 2. Unfortunately, faster scan rates than 250 mV/s could not be investigated due to high charging currents at 6 mm ITO electrodes. The fraction of active sites also depends on the scan rate, because the longer the experiment, the more time the metal complex has to find a guanine to oxidize. A second prediction that can be made is that as the number of guanines in the sequence is changed, the fraction of active sites (and its associated scan rate dependence) should vary in a well-defined manner. In particular, the fraction of active sites should be lower with DNA containing fewer guanines. This prediction cannot be tested using calf thymus DNA, which is always 20% guanine; however, the use of synthetic oligonucleotides allows complete sequence control and is now described.

CV of Oligonucleotides. The studies on calf thymus DNA do not reveal an explicit relationship between the fraction of active sites and the DNA sequence. In particular, effects of the number of guanines in the sequence and the proximity of those guanines to each other would be expected to change the fraction of active sites. CV experiments were therefore performed with oligonucleotides of known sequence. In all oligonucleotide sequences discussed here, the guanine is within an AGT sequence, since changes in the bases flanking the guanine can affect the redox potential in a sequence-dependent manner.[7,9,45,46] Although CV is not ideal for investigating biphasic reactions, the quantity of material required to observe the catalytic effect is much lower than in CA. Therefore, only CV experiments were performed on oligonucleotides, recognizing that the scan rate dependence is a necessary complication that arises from the biphasic nature of the catalysis apparent in Figure 2.

The first sequence investigated was a 15-mer oligonucleotide containing only one guanine, 5′-AAA-TAT-AGT-ATA-AAA-3′ (**G15**). Figure 5 shows the CV of $Ru(bpy)_3^{2+}$ with **G15**, which

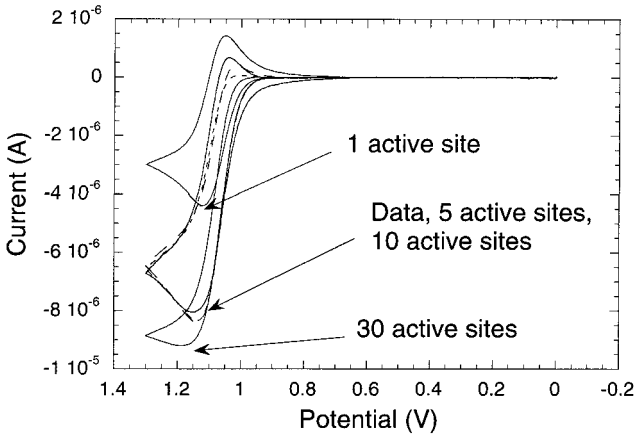

Figure 5. CV for 50 μM $Ru(bpy)_3^{2+}$ and **G15** (25 μM strand) at 100 mV/s (dashed). Solid lines show simulations calculated with 1, 5, 10, and 30 active sites.

exhibits a significant degree of catalytic current, *even though the concentration of guanine (25 μM) is smaller than that of the catalyst (50 μM)*. This observation highlights the importance of the binding equilibrium in enhancing the catalytic current and apparent rate constant. The data in Figure 5 are overlaid with a selection of simulations, each with optimized oxidation rate constants, over the entire range of active sites per strand. The case of only 1 active site represents the case where only binding at the single guanine in the sequence produces catalyst turnover. Clearly, much more catalysis is observed than predicted by this model. The other extreme is represented by 30 active sites, which corresponds to the case where binding anywhere on the oligonucleotide would result in catalyst turnover. The case of 30 active sites gives a sigmoidal voltammogram that exhibits the well-known $E_{rev}C'_{irrev}$ shape observed under true pseudo-first-order conditions.[34]

The data in Figure 5 are not fit well by either extreme case but instead suggest that binding of the metal complex at between 5 and 10 of the nucleotides in the oligomer leads to productive catalysis at 100 mV/s. For comparison to the calf thymus results, these values correspond to a fraction of active sites of 15−33%. This range is lower than that found for calf thymus DNA, which is expected since **G15** only contains 1 guanine out of 30 nucleotides while calf thymus DNA is 20% guanine. The complete set of optimal parameters at 100 mV/s for the digital simulations that fit the catalytic voltammograms of **G15** (Figure 5) are given in Table 3. Results are shown for the models corresponding to 10, 7.5, 6, and 5 active sites per duplex. As expected, the simulated first-order rate constants show a nearly linear dependence on the concentration of guanine added (Figure 6A), *and the second-order rate constants obtained via eq 5 are concentration-independent* (Figure 6B). The simulations clearly model the first-order nature of the electron-transfer step quite well since the second-order rate constants are concentration-independent. Further, the determined rate constant is not influenced by the active site fraction across this range of 5−10 active sites per duplex. The average rate constant determined from the 16 points in Table 3 is $(2.8 \pm 0.3) \times 10^5$ M^{-1} s^{-1}. This value is somewhat lower than that of 4.3×10^5 M^{-1} s^{-1} determined for calf thymus DNA at 100 mV/s in Table 2.

To further probe the origin of the active site fraction, oligonucleotides were investigated with greater numbers of guanines than in **G15**. To obtain satisfactory simulations of the voltammograms of 5′-AAA-AGT-AGT-AGT-AGT-AGT-AGT-AAA (**6G24**), at least 36 of the 48 nucleotides in the double-stranded oligomer were modeled as active. Simulation param-

TABLE 3: Digital Simulation Parameters for Oxidation of G15 at 100 mV/s

$[DNA]_t$ (μM)	$[G]_{exp}$ (μM)	active sites[a]	K_b^{3+} [b] (M^{-1})	k_1[c] (s^{-1})	$10^{-5} \times k_2$[d] ($M^{-1}\ s^{-1}$)
300	10	10	10500	5.5 (0.3)	2.8
300	10	7.5	14000	6.2 (0.3)	3.2
300	10	6	17500	6.5 (0.1)	3.3
300	10	5	21000	6.1 (0.2)	3.0
750	25	10	10500	8.2 (0.6)	2.4
750	25	7.5	14000	8.9 (0.7)	2.6
750	25	6	17500	9.4 (0.7)	2.7
750	25	5	21000	9.4 (0.6)	2.7
1500	50	10	10500	13.2 (0.6)	2.2
1500	50	7.5	14000	14.0 (0.7)	2.4
1500	50	6	17500	14.5 (0.7)	2.4
1500	50	5	21000	14.5 (0.7)	2.4
3000	100	10	10500	31.5 (1.6)	2.9
3000	100	7.5	14000	33.2 (2.0)	3.0
3000	100	6	17500	34.3 (2.5)	3.1
3000	100	5	21000	34.5 (3.0)	3.2

[a] Number of active sites per double-stranded oligonucleotide entered in these simulations. [b] Binding constant calculated from polyelectrolyte theory and adjusted for number of active sites in the model (see text). [c] First-order rate constant returned by digital simulation. [d] Second-order rate constant calculated according to eq 5.

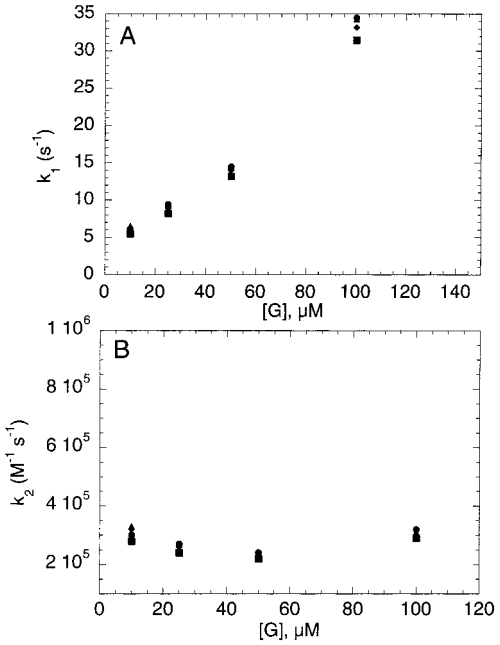

Figure 6. (A) First-order rate constants for oxidation of **G15** determined from simulation of CVs at 100 mV/s (as in Figure 5) for 5 (●), 6 (▲), 7.5 (◆), and 10 (■) active sites. (B) Second-order rate constants calculated from the data given in (A) using eq 5.

eters are given in Table 4, and as in the case of the **G15** sequence, the second-order rate constants were independent of the guanine concentration. Fitting of the data on the oligonucleotide **3G24**, with primary sequence 5′-AAA-TAT-AGT-AGT-AGT-TAT-ATA-AAA-3′, required a range of 6 to 36 active sites and gave rate constants very similar to those for **6G24** (Table 4). Finally, a series of three oligomers, each containing two guanines at different separations in a 48-base double helix, were used as substrates for the catalytic reaction. Fitting required a range of 6 to 24 active sites. Rate constants for the oligonucleotides containing two guanines (**2G2**, **2G8**, and **2G14**) are given in Table 4 and were similar to those for the other oligonucleotides. The separation of the guanines did not give an experimentally significant change in the simulated rate constant. In all cases, the second-order rate constants were independent of guanine concentration, and there was a modest but experimentally significant increase in the apparent rate constant as the scan rate was increased. The rate constants at 25 and 250 mV/s are shown for comparison in Table 4. As with calf thymus DNA, lower fractions of active sites were generally required at higher scan rates and the higher fractions gave better fits at lower scan rates.

Effect of Mediator Stereoisomers. The biphasic kinetics likely result from the existence of multiple, noninterconvertible binding modes that exhibit different electron-transfer kinetics.[47,48] Because $Ru(bpy)_3^{2+}$ can exist as both Δ and Λ stereoisomers and enantioselective interactions of chiral tris-chelate complexes with DNA are well-known,[49] we considered the possibility that the multiple kinetic processes stemmed from the presence of the two stereoisomers in the racemic mixtures of $Ru(bpy)_3^{2+}$ we had used up to this point. A racemic mixture of $Ru(bpy)_3^{2+}$ was resolved into the Δ and Λ isomers using standard techniques.[24] The catalytic currents obtained with the resolved Δ and Λ isomers were indistinguishable at high salt concentration and gave rate constants ($k_\Delta = 4900 \pm 300\ M^{-1}\ s^{-1}$; $k_\Lambda = 4500 \pm 400\ M^{-1}\ s^{-1}$) that were experimentally indistinguishable. Here, there is no appreciable binding of the $Ru(bpy)_3^{2+}$ to the DNA prior to electron transfer, so this experiment shows that the absolute rate constants for electron transfer in the DNA−$Ru(bpy)_3^{3+}$ encounter complex are identical. Further, Figure 7 shows that the catalytic currents for the two isomers are also indistinguishable at low salt concentration, where there is appreciable binding of the complex to DNA. Fitting of these data over multiple trials to the model in Scheme 1 again gives rate constants that are the same within the experimental error ($k_\Delta = 1.4 \pm 0.6 \times 10^5\ M^{-1}\ s^{-1}$ and $k_\Lambda = 2.6 \pm 1.3 \times 10^5\ M^{-1}\ s^{-1}$). Thus, any preference between the Δ and Λ isomers for binding to DNA does not influence the electron transfer rate. These results are consistent with those of numerous other workers in that stereoselectivity for binding, photochemistry, and electron transfer of DNA-bound tris(polypyridyl) complexes is generally observed *only* with much more sterically demanding complexes containing larger ligands such as 1,10-phenanthroline (phen), [49−51] 9,10-phenanthrenequinone diimine,[52,53] or dipyridophenazine.[54,55]

Discussion

Nature of the Biphasic Behavior. The observance of biphasic kinetics for the reactions of small molecules in the presence of DNA is quite common. Perhaps the most well-known such reactions are the simple emission decays of $Ru(bpy)_3^{2+}$ or $Ru(phen)_3^{2+}$ in the presence of DNA.[47,48] These complexes give monophasic emission decays in aqueous solution; however, biexponential emission decay is observed when some fraction of the complexes is bound to DNA.[47,48] This effect is even more pronounced when examining complexes with a higher affinity for DNA, such as $Ru(bpy)_2(dppz)^{2+}$, which exhibits a high DNA affinity and a biphasic emission decay.[55] This phenomenon has been ascribed to the existence of noninterconvertible subpopulations of the metal complexes bound to DNA in distinct conformations with different emission profiles. Accordingly, the emission decays show greater heterogeneity as the binding of the metal complex to DNA is increased.[47] Electron transfer reactions between many such bound complexes and DNA bases or other exogenous donors attached to DNA also show heterogeneous kinetics, presumably having a similar origin in multiple conformations of the donor−acceptor complex.[56,57] We show in Figure 7 that the biphasic kinetics observed here are not a result of the stereoisomerism

TABLE 4: Rate Constants as a Function of Guanine Fraction

name	sequence	simulated % active	actual %G	$k \times 10^{-5}$ (M^{-1} s^{-1}) (25 mV/s)	$k \times 10^{-5}$ (M^{-1} s^{-1}) (250 mV/s)
G15	5′-AAA-TAT-AGT-ATA-AAA	15−33%	3		
2G2	5′-AAA-TTA-TAT-AGT-AGT-ATA-ATT-AAA	12−50%	4	0.95	3.2
2G8	5′-AAA-TTA-AGT-ATA-TAT-AGT-ATT-AAA	12−75%	6.25	0.61	3.1
2G14	5′-AAA-AGT-ATA-TTA-TAT-ATT-AGT-AAA	12−75%	6.25	0.62	3.0
3G24	5′-AAA-TAT-AGT-AGT-AGT-TAT-ATA-AAA	12−75%	6.25	0.70	3.7
6G24	5′-AAA-AGT-AGT-AGT-AGT-AGT-AGT-AAA	75−100%	12.5	0.84	3.2
calf thymus	heterogeneous	60−100%	20	2.9	14

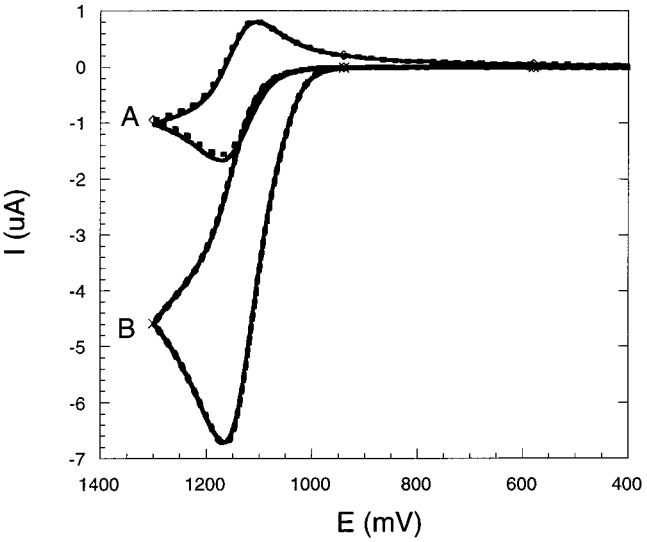

Figure 7. CVs of 50 μM Λ-Ru(bpy)$_3^{2+}$ (dashed) and Δ-Ru(bpy)$_3^{2+}$ (solid) (A) alone and (B) with 1 mM herring testes DNA.

of Ru(bpy)$_3^{2+}$, which is expected based on the low degree of stereoselectivity observed for bpy complexes in many other studies.[47,58]

The CA results in Figures 1 and 2 provide another example of biphasic kinetics for reactions of Ru(bpy)$_3^{2+}$ in the presence of DNA. In particular, at high ionic strength where there is no significant concentration of bound metal, the time dependence of the catalytic current is monophasic and exhibits a single rate constant in the purely kinetic regime described by eq 4. When the ionic strength is lowered, a significant amount of the metal complex is bound to DNA, presumably in multiple conformations, producing a biphasic time dependence for the catalytic current. The simplest explanation for this result, based particularly on past work on similar complexes,[47,48,59] is that a small fraction of the bound metal complexes is favorably oriented for electron transfer (and exhibit the fast decay). The majority of the complexes is then poorly oriented and must either dissociate and recollide with DNA or reorient while bound to achieve electron transfer. At high ionic strength, where all of the Ru(bpy)$_3^{3+}$ starts out in solution, all of the metal complexes can interconvert, whereas when binding occurs, the favorable metal complexes apparently cannot mix statistically with those that perform the slow electron transfer on the time scale of the reaction. The slow component in the bound case is about 10 times faster than the rate constant measured at high ionic strength (Table 1), which is the same difference observed by CV. This enhancement is due to an increase in local concentration of the metal complex brought about by DNA binding. The absolute rate constants for CA are somewhat smaller than those observed by CV for reasons discussed below.

Effect of Biphasic Behavior on CV. The ideal technique for analyzing the kinetics of a biphasic reaction such as that described here is one like CA that gives the entire kinetic trace for a process, revealing any biphasic behavior. In contrast, CV at a single scan rate only provides information on the first fraction of the reaction.[44] All of the CV results include contributions from the fast phase of the reaction, and the contribution of the slow phase becomes increasingly important as the scan rate is lowered. For this reason, the rate constants determined by CV decrease toward the value determined by CA as the scan rate is decreased. For example, the rate constant for calf thymus DNA determined by CV at 25 mV/s is 2.9×10^5 M^{-1} s^{-1} and increases to 1.4×10^6 M^{-1} s^{-1} at 250 mV/s. The range of rate constants determined from CA is 3.1×10^4 M^{-1} s^{-1} for the slow phase and 6.2×10^5 M^{-1} s^{-1} for the fast phase. Thus, the range of apparent rate constants from CV is narrower and somewhat faster than the range determined by CA. These differences probably occur because, at any scan rate, the fast component always contributes to the apparent rate in CV where the total kinetic process always contains the fast phase plus some amount of the slow phase that increases with decreasing scan rate. This effect narrows the range of apparent rate constants determined by CV and increases the absolute values determined.

DNA Binding Model. The DNA binding has a strong effect on the electrochemical response in both voltammetry and amperometry, enhancing the rate constant for electron transfer by roughly an order of magnitude. This effect is apparent both in rate constants returned from fitting of CV and in the simple slopes of the two linear regions in the CA, which are 1 and 2 orders of magnitude steeper than that observed at high salt. This enhancement must arise from a combination of factors that is apparently well simulated by increasing the effective DNA concentration from the concentration of guanine nucleotides to the concentration of active sites. The precise physical origins of the model probably lie in a combination of factors that includes diffusion of the mediator along the DNA strand,[59] dissociation and rebinding of the mediator during the electrochemical experiment,[60] and electron tunneling over multiple base pairs (i.e., at longer distances than just at the guanine nucleotide).[1,7−9]

Because of the effect of DNA binding, the sequence of the DNA is also important, particularly if there is a relatively small number of guanines in the sequence. For calf thymus DNA, where 20% of the nucleotides are guanine, many binding events lead to electron transfer, so the majority of the nucleotides in the sequence produce catalytic turnover upon binding Ru(bpy)$_3^{3+}$. In fact, our earlier simulations were for calf thymus DNA,[20] where we treated 100% of the nucleotides as active and were able to obtain acceptable fits. On the other hand, when guanines are scarce in the sequence, the effect of the sequence becomes important because there are many nucleotides that bind guanine and do not produce catalytic turnover. This effect is exemplified well by the data on the **G15** oligonucleotide, which we now consider in detail.

The DigiSim program allows calculation of the concentration profiles of the species in the reaction mechanism.[27] We have

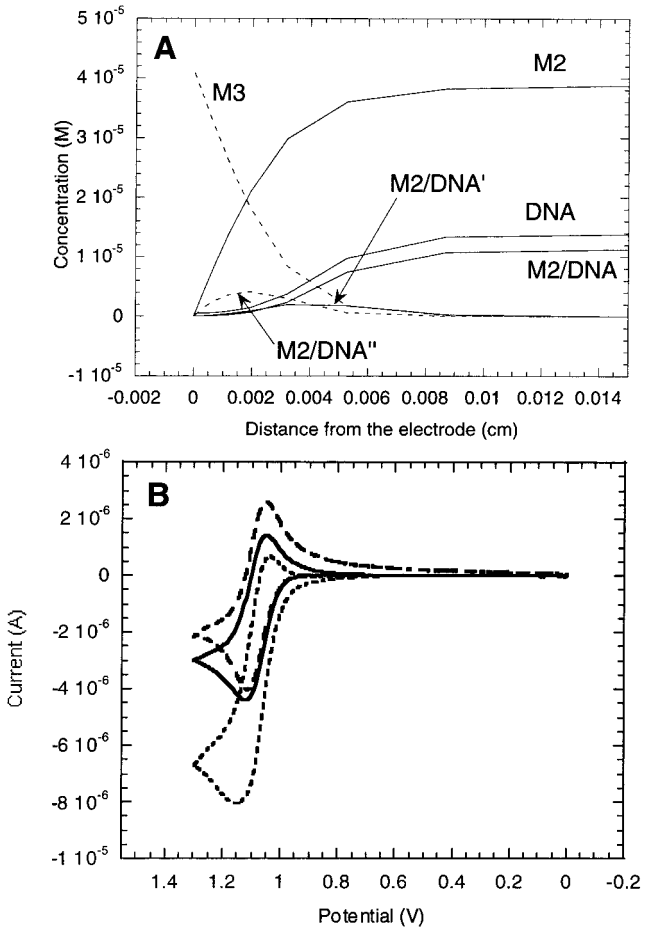

Figure 8. (A) Concentration profiles calculated at the switching potential for oxidation of **G15** using a model with one active site: M2 = $Ru(bpy)_3^{2+}$; M3 = $Ru(bpy)_3^{3+}$; M2/DNA = $Ru(bpy)_3^{2+}$·DNA; M2/DNA′ = $Ru(bpy)_3^{2+}$·DNA′; M3/DNA = $Ru(bpy)_3^{2+}$·DNA″. DNA concentration is the guanine concentration times the number of active sites. Scan rate = 100 mV/s. (B) CV calculated using the parameters from A (solid) and the experimental data (short dashed). The CV of $Ru(bpy)_3^{2+}$ alone is also shown (long dashed).

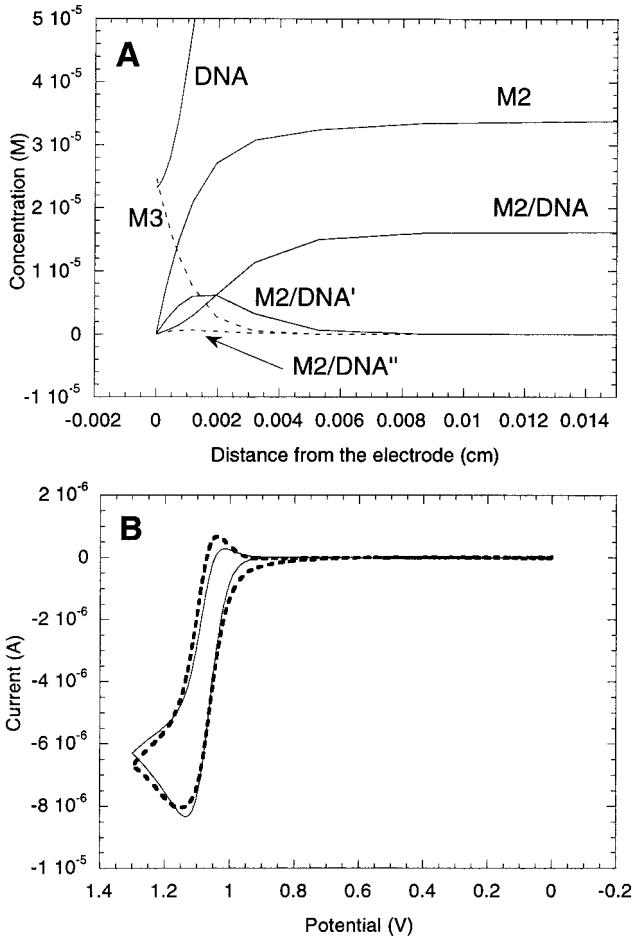

Figure 9. (A) Concentration profiles calculated at the switching potential for oxidation of **G15** using a model with 7.5 active sites. Scan rate = 100 mV/s. Abbreviations as in Figure 8. (B) CVs calculated using the parameters from A (solid) and the experimental data (dashed).

calculated these profiles at the switching potential (1.3 V) for simulations of the voltammetry for the **G15** oligonucleotide using models of 1, 7.5, and 30 active sites (Figures 8−10). These models correspond to the cases where only binding at the guanine nucleotide causes turnover (1 active site), binding to every nucleotide produces turnover (30 active sites), or an intermediate case. As shown in Figure 5, the intermediate case fits the data well, and modeling 5−10 active sites produces first-order rate constants that do not vary across this range of active sites and second-order rate constants that are independent of guanine concentration (Figure 6). We consider the concentration independence in Figure 6B to be strong validation of our model and assumptions, and we now consider the factors that produce this result in light of the concentration profiles in Figures 8−10.

Figure 8A shows the concentration profiles for the species in the model (Scheme 1) for the voltammogram calculated for one active site. In the Figure, the species M3 is unbound $Ru(bpy)_3^{3+}$, M2 is unbound $Ru(bpy)_3^{2+}$, M2/DNA is $Ru(bpy)_3^{2+}$ bound to DNA, M2/DNA′ is $Ru(bpy)_3^{2+}$ bound to DNA that has been oxidized once, and M2/DNA″ is $Ru(bpy)_3^{2+}$ bound to DNA that has been oxidized twice. The concentration of DNA given in the figure is actually that of the total DNA strand (25 μM in this case) times the number of active sites, which is the same as the DNA concentration since there is only one active site. The corresponding calculated voltammogram is shown in Figure 8B along with the experimental results for $Ru(bpy)_3^{2+}$ alone (long dashed) and $Ru(bpy)_3^{2+}$ with **G15** (short dashed).

As shown in the figure, the model with 1 active site predicts considerable depletion of DNA and M2/DNA at the electrode surface. As a result, the concentration of M3 at the electrode is nearly as high as would be expected in the absence of catalysis (the bulk concentration of $Ru(bpy)_3^{2+}$ is 50 μM), and there is an appreciable concentration of the two-electron product M2/DNA″ because most of the available DNA has undergone the first electron transfer early in the cycle and then gone on through the second electron transfer to generate M2/DNA″. In this case, the "best-fit" voltammogram gives little current enhancement compared to $Ru(bpy)_3^{2+}$ alone, the rate constant for the second electron transfer is significant compared to the rate constant for the first electron transfer, and the determined second-order rate constant is high compared to those determined at intermediate numbers of active sites. The rate constant is also a strong function of the DNA concentration. In summary, this model greatly underestimates the concentration of reactive nucleotides, so the model compensates by overestimating any rate constant that regenerates $Ru(bpy)_3^{2+}$. Even so, the model cannot generate catalytic current that approaches the experimental result.

Figure 9A shows the same concentration profiles as in Figure 8A for the case where there are 7.5 active sites. In this case, the DNA concentration in the model was 7.5 times the strand concentration (187.5 μM); hence, the DNA concentration is off-scale in Figure 9A except very close to the electrode surface. The DNA concentration is therefore larger than the $Ru(bpy)_3^{2+}$

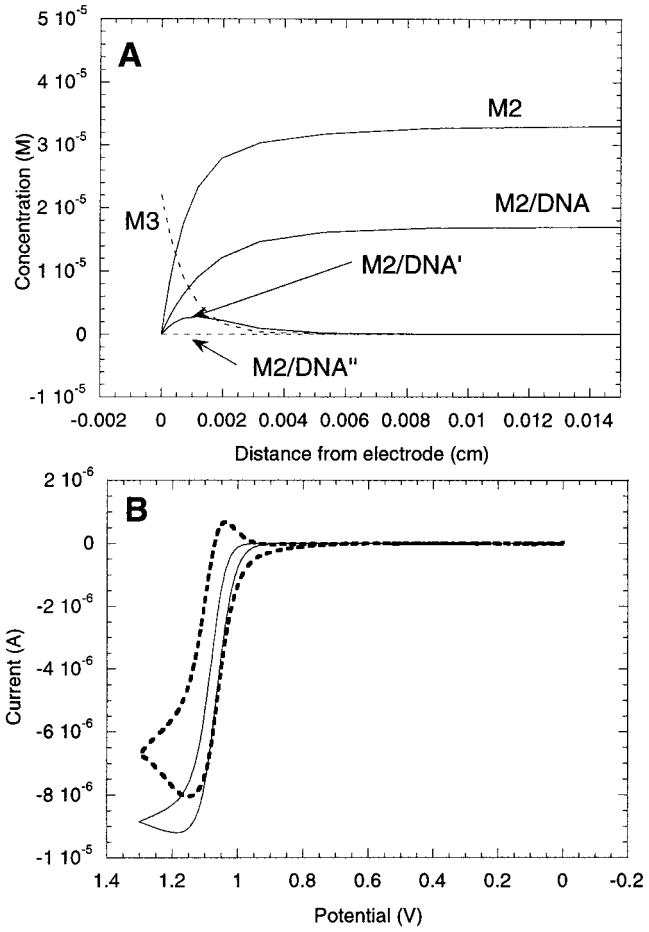

Figure 10. (A) Concentration profiles calculated at the switching potential for oxidation of **G15** using a model with 30 active sites. Scan rate = 100 mV/s. Abbreviations as in Figure 8. (B) CVs calculated using the parameters from A (solid) and the experimental data (dashed).

concentration (50 μM), but still not in a pseudo-first-order excess. The concentration profiles shown in Figure 9A show that in this model the M3 concentration at the electrode surface is significantly reduced compared to the bulk concentration of $Ru(bpy)_3^{2+}$. There is considerable depletion of M2/DNA at the electrode, but the concentration of the one-electron oxidation product (M2/DNA′) is significant at the electrode and depletes in the bulk, which is very different from the behavior seen in Figure 8A and indicates that the second electron-transfer process is not significant. The best-fit voltammogram (Figure 9B) was calculated with a rate constant for the second electron transfer that was small (<1%) compared to that for the first electron transfer. Accordingly, the M2/DNA″ concentration is insignificant. The experimental data show a considerable peak in the forward wave and a significant peak in the return direction, which are reasonably well simulated by the model.

Similar data for the model with 30 active sites are shown in Figure 10. The calculated voltammogram in Figure 10B shows somewhat more current enhancement than the intermediate case, but the shape of the voltammogram is much more sigmoidal, resembling a typical EC′-type voltammogram expected from a pseudo-first-order reaction.[34] With 30 active sites, the effective DNA concentration is now 750 μM, which is more than 10 times the $Ru(bpy)_3^{2+}$ concentration. Accordingly, the concentration profiles show a sharp increase in the M2/DNA concentration at the electrode, very little accumulation of M2/DNA′, and (as in Figure 9A) no significant concentration of M2/DNA″. The realization of true pseudo-first-order conditions compared to the intermediate case provides a relatively small gain in catalytic current at the oxidative peak (although considerably more at the switching potential), which is why observation of the catalytic effect is easiest with CV. At the time point of the peak current, the behavior for the intermediate case is apparently similar to that for the pseudo-first-order case. By the time the switching potential is reached, the lack of a pseudo-first-order excess has become more important, but by this point a relatively large signal has been measured at the peak potential.

When the density of guanine nucleotides in the DNA sequence is increased, the number of active sites also increases, as expected. As discussed above, the oligonucleotide with only 1 out of 30 guanine nucleotides behaves as though the guanine density were 5−10 times higher. As the actual guanine density is increased, the apparent density increases further, so that when DNA is composed of more than roughly 10% guanine, all of the nucleotides can be treated as active without changing the apparent rate constant (Table 4). This result is consistent with the order of magnitude increase in the apparent rate constants observed by both voltammetry and amperometry upon lowering the salt concentration.

Conclusions

A number of general points concerning guanine−$Ru(bpy)_3^{3+}$ electron transfer can be made from these results.

(1) We have a detailed picture of the kinetics at high salt where metal−DNA binding is not significant; the rate constants obtained by CV, CA, and stopped-flow spectrophotometry are in good agreement and are independent of DNA concentration.

(2) The reaction at low salt exhibits biphasic kinetics with rates that differ by roughly an order of magnitude. By CA, the corresponding second-order rate constants are independent of DNA concentration. By CV, the derived second-order rate constants are also independent of DNA concentration when fit to the model in Scheme 1. The biphasic kinetics are apparent in a dependence of the CV rate constants on scan rate. The biphasic kinetics are not a result of the stereoisomerism of $Ru(bpy)_3^{2+}$.

(3) The extraction of a second electron from guanine by another equivalent of $Ru(bpy)_3^{3+}$ is apparent in the CV, but the rate is much slower than that for the first electron transfer.

(4) When the guanine density is low, fitting of the CV data requires accounting for binding of the $Ru(bpy)_3^{2+}$ to the DNA in locations where electron transfer does not occur. Binding of the metal complex in the 2.5−5 basepair region containing the guanine leads to electron transfer.

Acknowledgment. This research was supported by Xanthon, Inc. and the National Science Foundation. M.F.S. thanks the Department of Education for a GAANN Fellowship. Numerous helpful discussions with Ivana Verona, Stephanie Codden, Paul Armistead, and Dr. Veronika Szalai concerning the development of the kinetic model are gratefully acknowledged.

References and Notes

(1) Henderson, P. T.; Jones, D.; Hampikian, G.; Kan, Y.; Schuster, G. B. *Proc. Natl. Acad. Sci. U.S.A.* **1999**, *96*, 8353−8358.

(2) Ratner, M. *Nature* **1999**, *397*, 480−481.

(3) Bernstein, R.; Prat, F.; Foote, C. S. *J. Am. Chem. Soc.* **1999**, *121*, 464−465.

(4) Beckman, K. B.; Ames, B. N. *J. Biol. Chem.* **1997**, *272*, 19633−19636.

(5) Kino, K.; Saito, I.; Sugiyama, H. *J. Am. Chem. Soc.* **1998**, *120*, 7373−7374.

(6) Duarte, V.; Muller, J. G.; Burrows, C. J. *Nucleic Acids Res.* **1999**, *27*, 496−502.

(7) Hall, D. B.; Holmlin, R. E.; Barton, J. K. *Nature* **1996**, *384*, 731−735.
(8) Lewis, F. D.; Wu, T.; Zhang, Y.; Letsinger, R. L.; Greenfield, S. R.; Wasielewski, M. R. *Science* **1997**, *277*, 673−676.
(9) Meggers, E.; Michel-Beyerle, M. E.; Giese, B. *J. Am. Chem. Soc.* **1998**, *120*, 12950−12955.
(10) Kelley, S. O.; Barton, J. K. *Science* **1999**, *283*, 375−381.
(11) Arkin, M. R.; Stemp, E. D. A.; Pulver, S. C.; Barton, J. K. *Chem. Biol.* **1997**, *4*, 389−400.
(12) Johnston, D. H.; Welch, T. W.; Thorp, H. H. *Metal Ions Biol. Syst.* **1996**, *33*, 297−324.
(13) Thorp, H. H. *Trends Biotechnol.* **1998**, *16*, 117−121.
(14) Wang, J.; Jiang, M.; Nilsen, T. W.; Getts, R. C. *J. Am. Chem. Soc.* **1998**, *120*, 8281−8282.
(15) Palecek, E. *Electroanalysis* **1996**, *8*, 7−14.
(16) Palecek, E.; Fojta, M. *Anal. Chem.* **1994**, *66*, 1566−1571.
(17) Singhal, P.; Kuhr, W. G. *Anal. Chem.* **1997**, *69*, 4828−4832.
(18) Johnston, D. H.; Cheng, C.-C.; Campbell, K. J.; Thorp, H. H. *Inorg. Chem.* **1994**, *33*, 6388−6390.
(19) Johnston, D. H.; Glasgow, K. C.; Thorp, H. H. *J. Am. Chem. Soc.* **1995**, *117*, 8933−8938.
(20) Johnston, D. H.; Thorp, H. H. *J. Phys. Chem.* **1996**, *100*, 13837−13843.
(21) Maniatis, T.; Fritsch, E. F.; Sambrook, J. *Molecular Cloning: A Laboratory Manual*, 2nd ed.; Cold Spring Harbor Press: Plainview, NY, 1989.
(22) Fasman, G. D. *CRC Handbook of Biochemistry and Molecular Biology*; CRC Press: Boca Raton, FL, 1975; Vol. 1.
(23) Kalyanasundaram, K. *Coord. Chem. Rev.* **1982**, *46*, 159−244.
(24) Rutherford, T. J.; Pellegrini, P. A.; Aldrich-Wright, J. A.; Junk, P. C.; Keene, F. R. *Eur. J. Inorg. Chem.* **1998**, 1677−1688.
(25) Armstrong, N. R.; Lin, A. W. C.; Fujihira, M.; Kuwana, T. *Anal. Chem.* **1976**, *48*, 741−750.
(26) Willit, J. L.; Bowden, E. F. *J. Phys. Chem.* **1990**, *94*, 8241−8246.
(27) Rudolph, M.; Reddy, D. P.; Feldberg, S. W. *Anal. Chem.* **1994**, *66*, 589a.
(28) Welch, T. W.; Thorp, H. H. *J. Phys. Chem.* **1996**, *100*, 13829−13836.
(29) Welch, T. W.; Corbett, A. H.; Thorp, H. H. *J. Phys. Chem.* **1995**, *99*, 11757−11763.
(30) Goinga, H. T.; Pecora, R. *Macromolecules* **1991**, *24*, 6128−6138.
(31) Kalsbeck, W. A.; Thorp, H. H. *J. Am. Chem. Soc.* **1993**, *115*, 7146−7151.
(32) Norden, B.; Lincoln, P.; Akerman, B.; Tuite, E. *Metal Ions Biol. Syst.* **1996**, *33*, 177−252.
(33) Creutz, C.; Sutin, N. *Proc. Natl. Acad. Sci. U.S.A.* **1975**, *72*, 2858−2862.
(34) Bard, A. J.; Faulkner, L. R. *Electrochemical Methods*; John Wiley and Sons: New York, 1980.
(35) Nicholson, R. S.; Shain, I. *Anal. Chem.* **1964**, *36*, 706−735.
(36) Yang, L.; Coury, L. A., Jr.; Murray, R. W. *J. Phys. Chem.* **1993**, *97*, 1694−1700.
(37) Manning, G. S. *Q. Rev. Biophys.* **1978**, *11*, 179.
(38) Manning, G. S. *Acc. Chem. Res.* **1979**, *12*, 443.
(39) Record, M. T., Jr.; Anderson, C. F.; Lohman, T. M. *Q. Rev. Biophys.* **1978**, *11*, 103.
(40) Kalsbeck, W. A.; Thorp, H. H. *Inorg. Chem.* **1994**, *33*, 3427−3429.
(41) Carter, M. T.; Rodriguez, M.; Bard, A. J. *J. Am. Chem. Soc.* **1989**, *111*, 8901.
(42) Doddridge, Z. A.; Cullis, P. M.; Jones, G. D. D.; Malone, M. E. *J. Am. Chem. Soc.* **1998**, *120*, 10998−10999.
(43) Steenken, S.; Telo, J. P.; Novais, H. M.; Candeias, L. P. *J. Am. Chem. Soc.* **1992**, *114*, 4701−4709.
(44) Osteryoung, J. *Acc. Chem. Res.* **1993**, *26*, 77−83.
(45) Saito, I.; Takayama, M.; Sugiyama, H.; Nakatani, K.; Tsuchida, A.; Yamamoto, M. *J. Am. Chem. Soc.* **1995**, *117*, 6406−6405.
(46) Gasper, S. M.; Schuster, G. B. *J. Am. Chem. Soc.* **1997**, *119*, 12762−12771.
(47) Kumar, C. V.; Barton, J. B.; Turro, N. J. *J. Am. Chem. Soc.* **1985**, *107*, 5518−5523.
(48) Pyle, A. M.; Rehmann, J. P.; Meshoyrer, R.; Kumar, C. V.; Turro, N. J.; Barton, J. K. *J. Am. Chem. Soc.* **1989**, *111*, 3051−3058.
(49) Barton, J. K.; Goldberg, J. M.; Kumar, C. V.; Turro, N. J. *J. Am. Chem. Soc.* **1986**, *108*, 2081−2088.
(50) Satyanarayana, S.; Dabrowiak, J. C.; Chaires, J. B. *Biochemistry* **1992**, *31*, 9319.
(51) Satyanarayana, S.; Dabrowiak, J. C.; Chaires, J. B. *Biochemistry* **1993**, *32*, 2573−2584.
(52) Pyle, A. M.; Long, E. C.; Barton, J. K. *J. Am. Chem. Soc.* **1989**, *111*, 4520.
(53) Sitlani, A.; Dupureur, C. M.; Barton, J. K. *J. Am. Chem. Soc.* **1993**, *115*, 12589−12560.
(54) Haq, I. L., P.; Chaires, J. B. *J. Am. Chem. Soc.* **1995**, *117*, 4788.
(55) Jenkins, Y.; Friedman, A. E.; Turro, N. J.; Barton, J. K. *Biochemistry* **1992**, *31*, 10809.
(56) Arkin, M. R.; Stemp, E. D. A.; Turro, C.; Turro, N. J.; Barton, J. K. *J. Am. Chem. Soc.* **1996**, *118*, 2267−2274.
(57) Arkin, M. R.; Stemp, E. D. A.; Holmlin, R. E.; Barton, J. K.; Hörmann, A.; Olson, E. J. C.; Barbara, P. F. *Science* **1996**, *273*, 475−480.
(58) Barton, J. K.; Dannenberg, J. J.; Raphael, A. L. *J. Am. Chem. Soc.* **1982**, *104*, 4397−4969.
(59) Barton, J. K.; Kumar, C. V.; Turro, N. J. *J. Am. Chem. Soc.* **1986**, *108*, 6391−6393.
(60) Carter, M. J.; Bard, A. J. *J. Am. Chem. Soc.* **1987**, *109*, 7528−7530.